GEO-LEO Reflective Band Inter-comparison with BRDF and Atmospheric Scattering Corrections

Tiejun Chang[a], Xiaoxiong Xiong[b], Graziela R. Keller[a], and Xiangqian Wu[c]

[a] Science Systems and Applications, Inc., Lanham, MD 20706

[b] Sciences and Exploration Directorate, NASA/GSFC, Greenbelt, MD 20771

[c] NOAA/NESDIS/STAR, College Park, MD 20740

ABSTRACT

The inter-comparison of the reflective solar bands (RSB) between the instruments onboard a geostationary orbit satellite and a low Earth orbit satellite is very helpful in assessing their calibration consistency. Himawari-8 was launched 7 October 2014 and GOES-R was launched on 19 November 2016. Unlike previous GOES instruments, the Advanced Himawari Imager (AHI) on Himawari-8 and the Advanced Baseline Imager (ABI) on GOES-R have onboard calibrators for the RSB. Independent assessment of calibration is nonetheless important to enhance their product quality. MODIS and VIIRS can provide good references for sensor calibration.

In this work, the inter-comparison between AHI and VIIRS is performed over a pseudo-invariant target. The use of stable and uniform calibration sites provides comparison with accurate adjustment for band spectral difference, reduction of impact from pixel mismatching, and consistency of BRDF and atmospheric correction. The site used is the Strzelecki Desert in Australia. Due to the difference in solar and view angles, two corrections must be applied in order to compare the measurements. The first is the atmospheric scattering correction applied to the top of atmosphere reflectance measurements. The second correction is applied to correct the BRDF effect. The atmospheric

correction is performed using a vector version of the Second Simulation of a Satellite Signal in the Solar Spectrum (6SV) model and the BRDF correction is performed using a semi-empirical model. Our results show that AHI band 1(0.47 μm) has a good agreement with VIIRS band M3 within 0.15%. AHI band 5 (1.61 μm) shows the largest difference (5.09%) with VIIRS band M10, while AHI band 5 shows the least difference (1.87%) in comparison with VIIRS band I3. The methods developed in this work can also be directly applied to assess GOES-16/ABI calibration consistency, a topic we will address in the future.

Keywords: Inter-comparison, Radiometric calibration, BRDF, MODIS, VIIRS, Himawari-8, GOES-16, GOES-R

1. INTRODUCTION

The Japan Meteorological Agency (JMA) Himawari-8 spacecraft was launched on 7 October 2014 and began operations in July 2015 [1]. The US National Oceanic and Atmospheric Administration (NOAA) GOES-16 (known as GOES-R before launch) satellite was launched in 19 November 2016 [2]. They carry the Advanced Himawari Imager (AHI) and Advanced Baseline Imager (ABI), respectively. AHI and ABI both have six reflective solar bands. Comparing with the previous imagers onboard geostationary satellites, AHI and ABI provide higher spatial resolution and enhanced radiometric calibration accuracy for a full disk image of the Earth acquired every 10 minutes and every 15 minutes, respectively. The inter-comparison between satellite sensors over vicarious calibration sites can provide valuable information for the instrument calibration and uncertainty assessments. For geostationary (GEO) satellite sensors, such as AHI and ABI, the inter-comparison with Low Earth Orbiting (LEO) satellite sensors, such as the Moderate Resolution

Imaging Spectroradiometer (MODIS) and the Visible Infrared Imager Radiometer Suite (VIIRS), can enhance the calibration accuracy. However, for the reflective solar bands (RSB), a major challenge in cross-sensor comparison of instruments on different satellites is the differences in solar and view angles of their measurements over a given pseudo-invariant site. Observations from simultaneous nadir overpasses (SNO) and ray matching between two sensors have been used to reduce these effects [3-6]. Both Himawari-8 and GOES-16 are located above tropical ocean regions. When using the ray-matching technique, the observations may be from different types of targets and the radiance levels may not cover the desired range.

In this study, a method for GEO-LEO inter-comparison of RSBs over a selected pseudo-invariant site was developed. Two corrections have been applied to the reflectance measurements over the site. The satellite sensor measures the top of the atmosphere (TOA) reflectance. The atmospheric scattering (primarily Rayleigh) has a significant impact on the retrieved TOA reflectance, especially at short wavelengths. A correction for the atmospheric scattering effect is performed using a vector version of the Second Simulation of a Satellite Signal in the Solar Spectrum - Vector (6SV) model [7-10]. After correcting for the atmosphere scattering and transmittance, the surface reflectance is retrieved. Then a semi-empirical Bidirectional Reflectance Distribution Function (BRDF) model is used to correct the ground reflectance [11]. For a GEO sensor, measurements over a selected site have a fixed view angle and modeling the BRDF using limited view angle coverage will introduce bias in the BRDF coefficients. In this work, the BRDF is modeled using one-year of LEO measurements for each selected reflectance band with broad coverage of solar angles. The BRDF correction is applied to the matching bands of both LEO and GEO sensors.

The demonstration in this paper focuses on the comparison between AHI and VIIRS. The BRDF is surface type dependent and a spatially homogeneous scene is desirable to have a uniform BRDF effect over the selected site and over time. The most frequently used calibration sites, such as the Libya deserts, are not in the score of AHI observations. A desert site in Australia (latitude 29.0 South; longitude 139.8 East) was selected as the pseudo-invariant calibration site for being spectrally and temporally uniform [12]. VIIRS and AHI have a total of 9 spectral matching band pairs. VIIRS passes the selected site once a day, while AHI provides full disk measurements every 10 minutes and a large number of samples for the inter-comparison.

Section 2 provides background on the two instruments and correction models. The inter-comparison methodology is presented in section 3 including the 6SV model, the BRDF model, and the spectral band adjustment factor (SBAF). The comparison algorithm and a detailed flow chart are also presented. Section 3 shows the corrections to the AHI reflectance and the comparison results for its 6 RSB bands with VIIRS matching bands, as listed in Table 1 in section 3.1. The data used in the comparison are the VIIRS sensor data record (SDR) product and AHI level 1 B (L1B) product in year 2016.

2. BACKGROUND

2.1 Instruments

SNPP/VIIRS was launched on 28 October 2011. It has 14 reflective bands, M1-M11 and I1-3, covering 0.4-2.2 μm and 7 emissive bands, M12-16 and I4-5, covering 3.7-12 μm. The spatial resolution at nadir is 750 m for the 16 moderate resolution radiometric bands (M bands) and 375 m for the 5 imaging bands (I bands) [13, 14]. Each M band consists of 16 detectors. Each I band

consists of 32 detectors. Bands M1 to M5 and M7 have a dual gain capability to cover a larger radiometric dynamic range. Bands M7 and I2 and bands M10 and I3 are designed to have same spectral response respectively. The VIIRS calibration uses an on-board solar diffuser (SD) and its SD degradation is monitored using a SD stability monitor (SDSM). Lunar observations are also used for instrument gain trend monitoring and correction.

The Himawari-8 spacecraft, which was launched on 7 October 2014 and with a suborbital point longitude of ~140.7 º east, covers the East Asia and Western Pacific regions. The primary instrument aboard Himawari-8, AHI, is a 16-channel multispectral imager which captures visible light and infrared images of the Asia-Pacific region [1]. Among the 16 channels, channels 1-3 cover the visible spectral range and 4-6 are near-infrared bands with spatial resolutions from 0.5 km to 2 km at nadir. The instrument has similar spectral and spatial characteristics to ABI on the GOES-16 satellite. AHI produces full disk observations every 10 minutes while ABI produces full disk observations every 15 minutes. Both AHI and ABI instruments feature higher spatial, spectral, and radiometric resolution than previous imagers onboard geostationary satellites. The RSB calibration uses an on-board SD for both AHI and ABI.

2.2 Correction models

2.2.1 Atmospheric correction

The satellite sensors retrieve the TOA reflectance. The atmospheric correction implemented in this work uses the 6SV model. The 6SV model uses a basic radiative transfer model to calculate the atmospheric correction. It facilitates accurate simulations of satellite observations [7-10]. It is used in this work for the characterization of the atmospheric scattering effects, especially Rayleigh

scattering at short wavelengths. For satellite sensor over uniform targets, such as the selected desert site, the TOA reflectance includes both transmitted ground reflectance and atmospheric scattering. For a given spectral band of satellite sensor and given scene parameters, the TOA reflectance and scattering at certain solar and view angles over a selected scene can be derived from ground reflectance [10],

$$R_{TOA}(\theta_s,\theta_v,\phi) = R_{scattering}(\theta_s,\theta_v,\phi) + \frac{R_t}{1-R_tS}T(\theta_s)T(\theta_v) \quad (1)$$

where $\theta_{s(v)}$ are solar zenith or view zenith angle, ϕ is the relative azimuth angles, $R_{scattering}(\theta_s,\theta_v,\phi)$ is scattering with solar and view angle dependencies, S is the spherical albedo of the atmosphere, $T(\theta_s)$ and $T(\theta_v)$ are downward and upward transmittances. R_t in Eq. (1) is the target reflectance. The 6SV model is used to derive the ground reflectance and Rayleigh scattering for uniform desert site. Both the ground reflectance and the scattering are dependent on solar and view angles. The site BRDF affects the ground reflectance. The 6SV manual describes a scheme for the atmospheric correction [7-10].

2.2.2 BRDF correction

As the reflectance measurements are taken at different solar and view angles, a BRDF model needs to be applied to correct for bidirectional effects. In this work, a semi-empirical model is used for the BRDF correction. The BRDF is scene dependent and, for a pseudo-invariant desert site, the BRDF coefficients are assumed to be homogeneous and stable. A semi-empirical model developed by Roujean et al. is widely used to correct the bidirectional effect on the reflectance and the model coefficients are adjustable to account for the variations in surface type [11]. The model coefficients

are adjustable to account for the variations in surface type, where the surface reflectance is expressed as

$$R(\theta_s,\theta_v,\phi) = k_0 + k_1 f_1(\theta_s,\theta_v,\phi) + k_2 f_2(\theta_s,\theta_v,\phi) \quad (2)$$

where

$$f_1(\theta_s,\theta_v,\phi) = \frac{1}{2\pi}\left[(\pi-\phi)\cos\phi + \sin\phi\right]tan\theta_s tan\theta_v ,$$

and

$$f_2(\theta_s,\theta_v,\phi) = \frac{4}{3\pi}\frac{1}{\cos\theta_s + \cos\theta_v}\left[\left(\frac{\pi}{2}-\xi\right)\cos\xi + \sin\xi\right] - \frac{1}{3}$$

The solar angle and view angle ranges, the sample size, the variation in reflectance retrieval conditions, and sensor reflectance measurement bias may affect the precision of these coefficients. GEO satellites have a fixed view angle over a selected site and the BRDF modeling using measurements from a GEO instrument may present difficulties when applied to other instruments. The LEO satellite provides a broad range of solar and view angles, especially when one-year of measurements are used. The BRDF coefficients from a LEO instrument can be applied to the measurements from a GEO instrument. On the other hand, the GEO instrument provides Earth full disk images within a short time period for AHI (10 minutes). The large number of samples over the calibration site provides a larger range of solar angles, and can be used for BRDF modeling verification.

2.2.3 SBAF

For a comparison between reflectance measurements of spectral matching bands of two instruments, a correction should be used to account for the spectral response differences between them. The intrinsic offsets between two sensors caused by spectral response function (SRF) mismatches can be compensated for by using a spectral band adjustment factor (SBAF), which takes into account the spectral profile of the target and the SRF of the two sensors. A SBAF can be derived based on visible hyper-spectral data from numerical modeling or from hyper-spectral measurement data over the selected target [15, 16]. In this work, MODerate resolution atmospheric TRANsmission (MODTRAN) 5.2.1 was used to simulate the bandpass radiance measurements over a typical desert site [17].

3. METHOD DEVELOPMENT

3.1 Spectral matching bands

The matching bands for VIIRS and AHI are listed in the table 1 and their SRFs are shown in the plots of Figure 1. All 6 AHI RSBs have been matched with VIIRS bands. The SRFs of VIIRS M7 and I2 are similar, which have good matching with AHI 0.86 μm band. However I bands have higher spatial resolution and these two VIIRS bands are calibrated independently. Similarly, VIIRS bands M10 and I2 have good spectral matching with AHI 1.60 μm band. Overall VIIRS I bands have better matching than M bands due to their comparable spectral bandwidth with AHI bands. VIIRS band M3 is used for comparison with AHI 0.47 μm and 0.51 μm bands. However, the spectral differences for these two pairs are larger compared to the other band pairs. The SBAF is used for the correction of the spectral differences between the matching band pairs.

Table 1. The matching band pairs between AHI and VIIRS.

AHI Band Wavelength (μm)	0.47	0.51	0.64	0.86	1.61	2.20
VIIRS M band	M3	M3	M5	M7	M10	M11
M band wavelength (μm)	0.49	0.49	0.67	0.86	1.61	2.25
VIIRS I band			I1	I2	I3	
I band wavelength (μm)			0.64	0.86	1.61	

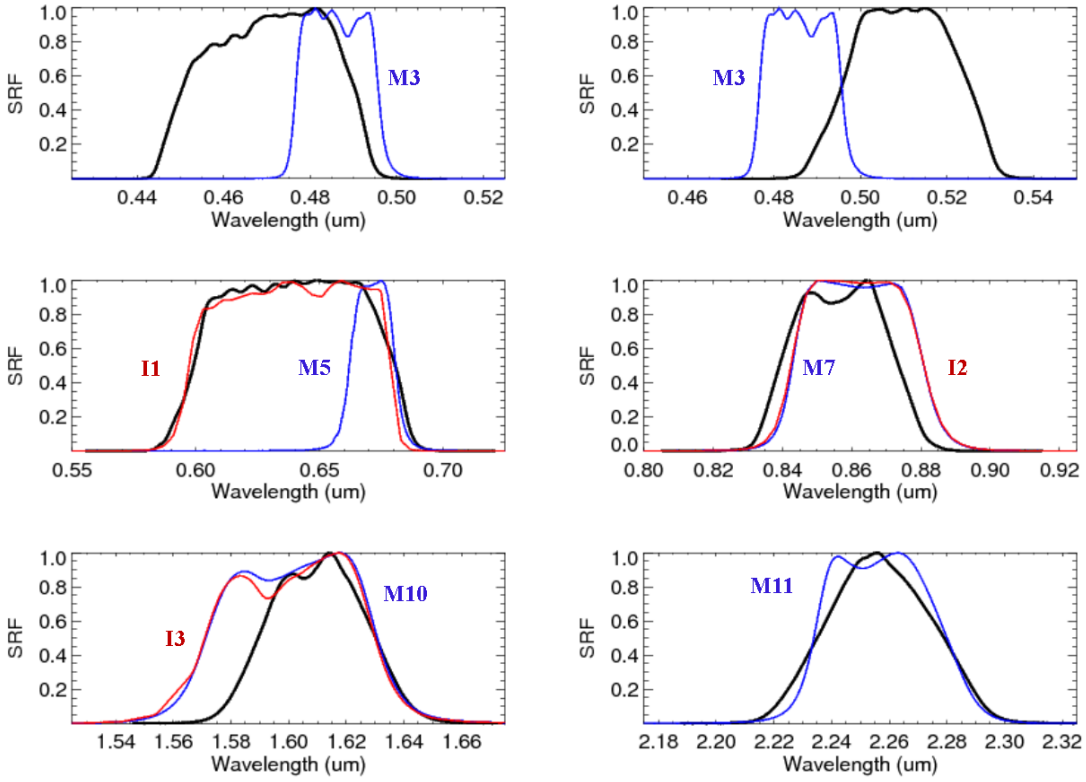

Figure 1. The SRFs of the matching band pairs of AHI and VIIRS are plotted for comparison. The AHI band spectral response functions are plotted in black. Blue curves denote VIIRS M bands and red curves denote VIIRS I bands.

3.2 Comparison site

When selecting the comparison site, the geolocation error and pixel mismatch should be considered and the site should ideally be uniform. The stability of the BRDF and of the atmospheric correction should also be considered. The instrument view angle can also have an effect on the measurements. Using the nadir pixels would enhance the comparison accuracy. However, Himawari-8 is located over a very low reflectance ocean site, which is not appropriate for RSB inter-comparison. In our previous works for LEO-LEO inter-comparison with BRDF and atmospheric corrections, the most common calibration sites are Libyan deserts [18, 19]. As Himawari-8 AHI covers the East Asia and Western Pacific regions, the Libyan deserts cannot be used in this work. In this work, the Strzelecki Desert site in Australia was selected for the inter-comparison [12]. Figure 2 shows the site and the location of Himawari-8 on a map and lists the site coordinates and VIIRS passing time in day time. Due to its geostationary orbit, the zenith angle for AHI is fixed at 33.8 º. The AHI data used for the comparison encompasses 24 measurements each day from 2:00 to 5:50 UTC (11:00 to 14:50 local time).

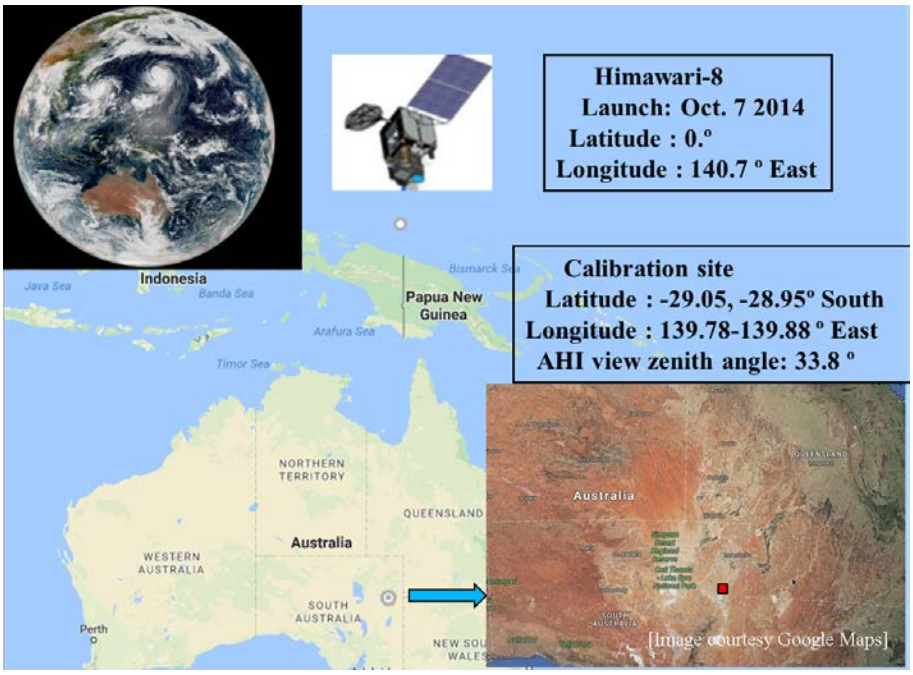

Figure 2. The himawari-8 location and calibration site location on map [1].

3.3 Solar and view angle coverage

For accurate BRDF modeling, a sufficient sample size covering broad ranges of solar and view angles is required. VIIRS 2016 one-year measurements over the selected calibration site are used. Since AHI has a fixed view angle over the selected site, the use of AHI measurements over the site may induce errors in the BRDF coefficients. The left plot in Figure 3 shows the range of solar and view angles covered by the selected VIIRS data. To separate the view angles relative to nadir in the plot, one side of nadir is defined as negative sensor zenith angle. The view angle with frame number less than that of the nadir frame is defined as a negative view angle while the remaining frames are defined as positive view angles. The VIIRS sensor zenith angle covers up to 60º on each side. The solar zenith angle, on the other hand, varies from 10º to 60º. The relative azimuth angle is defined as the angle between the solar azimuth and sensor azimuth vectors [10, 11]. For a LEO sensor, the

relative azimuth angle for one side of nadir is less than 90º, while larger than 90º for the other side. For VIIRS, a negative view angle corresponds to less than 90º of relative azimuth angle, while the other side has relative azimuth angle larger than 90º. The AHI data selected includes 24 measurements each day and the data from 2016 covers solar zenith angles from 5º to 60º, as shown in the right plot in Figure 3 for comparison. The horizontal axis is the time difference between the observations of the target by the two instruments.

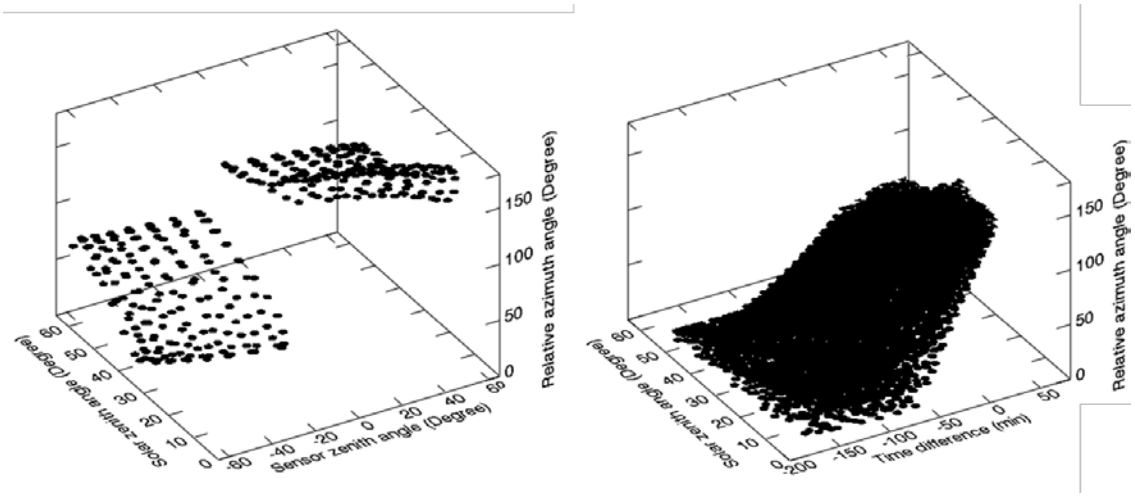

Figure 3. (Left) VIIRS solar and view angle coverage for 2016 measurements over the selected site. (Right) AHI solar angle coverage for 2016 measurements over the selected site. AHI has a fixed sensor zenith angle of 33.8 º.

3.4 Atmospheric correction

Figure 4 shows the TOA reflectance from VIIRS band M3 measurements over the selected site. The TOA reflectance varies with both solar and view angles. The angle dependencies are significant. The TOA reflectance data for all matching bands should be corrected for atmospheric scattering and the BRDF effect. The reflectance ranges from 0.18 to 0.28. The variation is due to the angle dependence

of atmospheric scattering and BRDF effect of the ground reflectance. Since the BRDF model is for ground reflectance, the atmospheric scattering and the ground reflectance must be derived before applying the BRDF model.

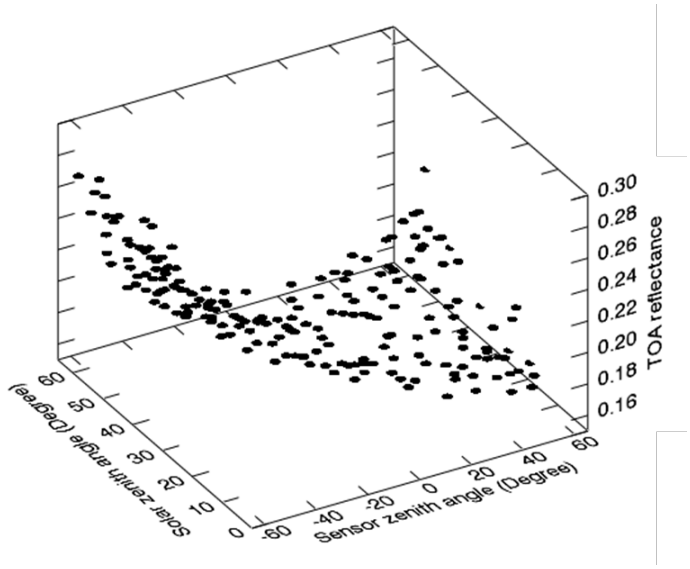

Figure 4. TOA reflectance measurements from VIIRS band M3 as function of solar and view angles. The measurements are from 2016 over the selected site.

The 6SV model was used to derive the Rayleigh scattering and ground reflectance over uniform desert scene for a given solar zenith angle, view zenith angle, relative azimuth angle, and reflectance [10]. Figure 5 shows the modeled Rayleigh scattering and the normalized Rayleigh scattering which is defined as the ratio of the Rayleigh scattering to TOA reflectance. The Rayleigh scattering varies with solar and view angles. The signal ratio is also dependent on the angles. The Rayleigh scattering ranges from 0.02 to 0.06 as shown in the left plot of Figure 5. The ratio ranges from 0.12 to 0.22, as shown in the right plot of Figure 5. The atmospheric scattering has a significant effect on the inter-comparison and the correction is necessary.

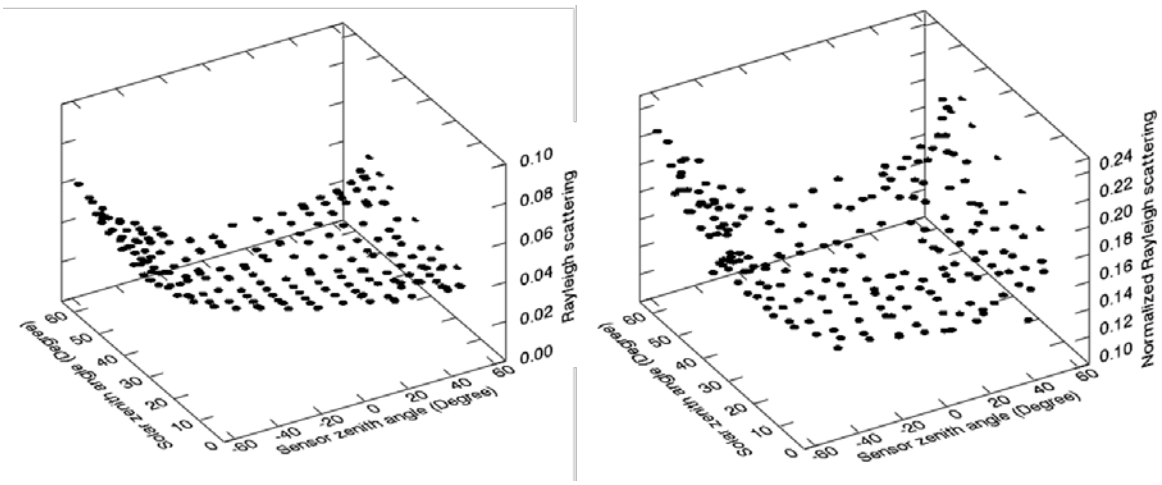

Figure 5. (Left) Rayleigh scattering as function of solar and view angles for VIIRS band M3 from one-year of measurements (2016) over the selected site. (Right) The ratio of the Rayleigh scattering to TOA reflectance for M3.

3.5 BRDF correction

The ground reflectance derived from atmospheric scattering correction still depends on the solar zenith angle, the view zenith angle, and the relative azimuth angle due to the site's BRDF. The left plot of Figure 6 shows the VIIRS band M3 ground reflectance as a function of the solar zenith angle and the sensor zenith angle. The atmospheric scattering has larger effect on short wavelength band and the pair of AHI 0.47 μm band and VIIRS M3 is the shortest bands in this comparison. This plot does not show the exact dependence on relative azimuth angle. However, since the sign of view zenith angle indicates the range of relative azimuth angles, the reflectance dependence on the sign of the view zenith angle can represent some effect of relative azimuth angle. The ground reflectance of each matched VIIRS RSB is used in the regression to derive the BRDF over the selected site using the BRDF model [11]. The plot in the right panel of Figure 6 shows the ground reflectance from the

BRDF modeling. The BRDF coefficients will be used to make the reflectance correction for both VIIRS and AHI reflectance.

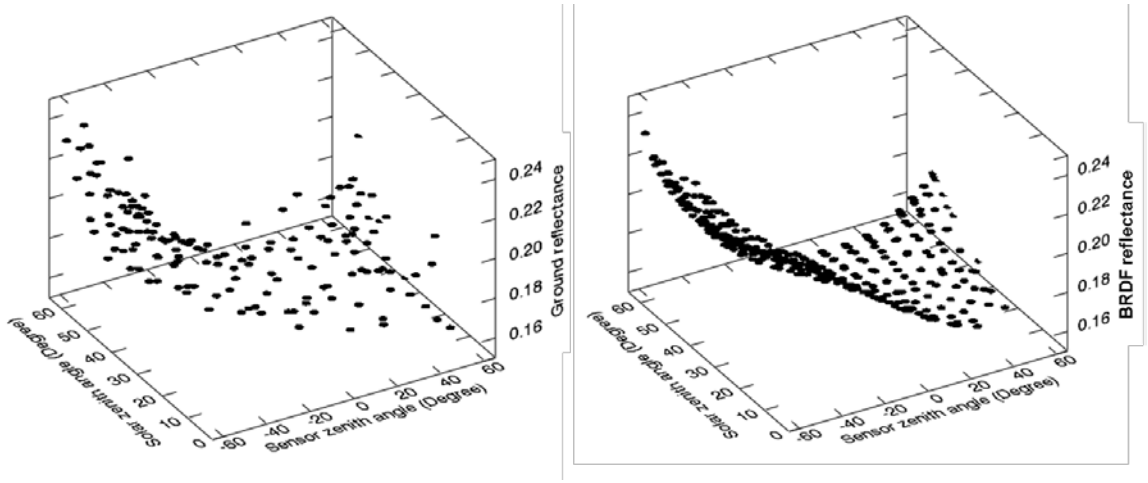

Figure 6. (Left) Ground reflectance as function of solar and view angles for VIIRS band M3 from one-year of measurements (2016) over the selected site. (Right) The ground reflectance from the BRDF model for VIIRS band M3.

4. COMPARISON

4.1 Contamination removal

The corrections presented in section 3 were implemented in the comparison between VIIRS and AHI. The reflectance after atmospheric scattering and BRDF corrections are used for comparison. The same parameters and coefficients for both corrections are applied and it requires the scene to be uniform and stable. However, the Strzelecki Desert site may have cloud contamination and contaminated measurements should be removed from the comparison. The cloud presence can be

identified from the site uniformity, reflectance level, and reflectance stability over time. Figure 7 shows the identification of contaminated measurements. The data points in blue were identified as contaminated measurements and filtered out, while the data points in red are the measurement used for the comparison.

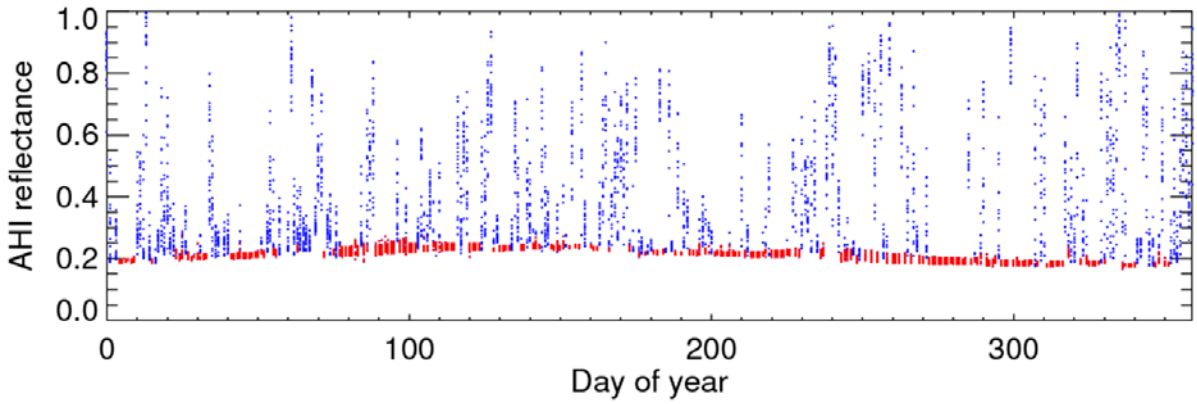

Figure 7. AHI band 1 TOA reflectance measurements during 4 hour time and over the selected site. The data points in blue were identified as contaminated measurements.

4.2 Comparison implementation

The measurements after removing the cloud contamination are used for modeling and comparison. The left plot of Figure 8 shows the ground reflectance as a function of solar and view angles for VIIRS M3 from 2016 measurements over the selected site. The broad coverage of solar and view angles can enhance the BRDF modeling accuracy. The BRDF modeling from a VIIRS band using one year of data is used to correct each measurement of that band as well as the matched AHI band. The right plot shows the BRDF corrected ground reflectance of each measurement for VIIRS M3

using the BRDF coefficients for that band. Ideally, there should be no solar and view angle dependence once the corrections have been applied.

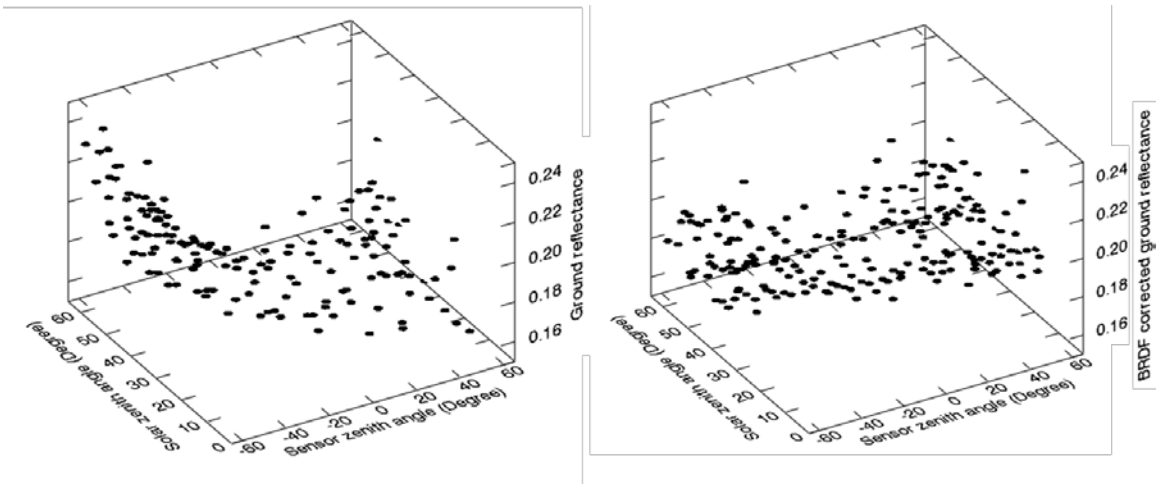

Figure 8. (Left) Ground reflectance as a function of solar and view angles for VIIRS band M3 from 2016 measurements over the selected site. (Right) The BRDF corrected ground reflectance of each measurement for VIIRS M3.

The flow chart in Figure 9 illustrates the procedure for the atmospheric scattering correction, BRDF modeling, and comparison. The VIIRS ground reflectance after the atmospheric scattering correction is used in the regression to derive the coefficients for the BRDF model and then each ground reflectance is corrected using the BRDF coefficients. The atmospheric scattering correction and BRDF was also applied to every AHI reflectance measurement. The comparison between AHI and VIIRS measurements is performed as a day-to-day difference of corrected reflectance. The day-to-day difference reduces the effect of target contamination and seasonal variation. AHI produces full disk observations every 10 minutes, while VIIRS observes the site once a day from 3:36 to 5:18

UTC (12:36 to 14:18 local time). AHI measurements in the time range of 2:00 to 5:50 UTC (11:00 to 14:50 local time) were analyzed. The multiple AHI measurements can be used to verify the correction accuracy and to remove any additional dependence due to band spectral differences. The 4-hour time period can provide the variation of solar angle in addition to the seasonal variation. The differences between daily VIIRS measurement with the same day 24 measurements from AHI were calculated. The observation time difference between the measurements of the two instruments was also processed and its effect was also considered in the comparison.

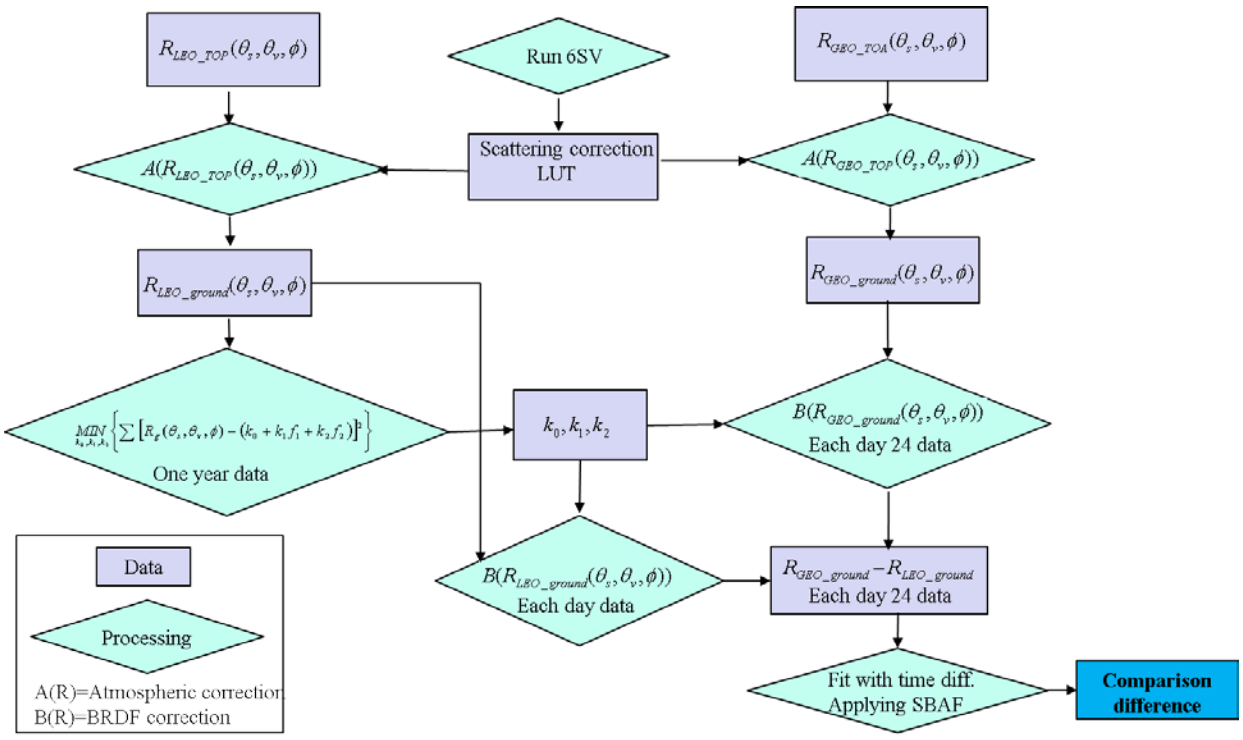

Figure 9. The flow chart for corrections and comparison between VIIRS and AHI for each matching band pair.

The 4 hour time period of AHI measurements provides daily variation in the solar angle in addition to seasonal variation. The top plot of Figure 10 shows AHI solar zenith angles as a function of measurement time for VIIRS over the selected site. The solar angle range is broad, from approximately 8º to 70º. The bottom plot shows the AHI relative azimuth angle as function of measurement time for VIIRS over the selected site; it ranges from 0º to 90º. If the corrections of atmospheric scattering and BRDF are perfect and the site reflectance is stable, there should be no dependence of the reflectance difference on the observation time difference. In reality, the correction models are not perfect and can induce systematic error. These deficiencies can contribute bias to the comparison. However, this bias is expected to be reduced as observation time difference since the effects from solar zenith angles are canceled in the comparison. An empirical function is applied for the comparison with the observation time difference. The reflectance difference calculated with the empirical function at zero time difference is used as the results of comparison.

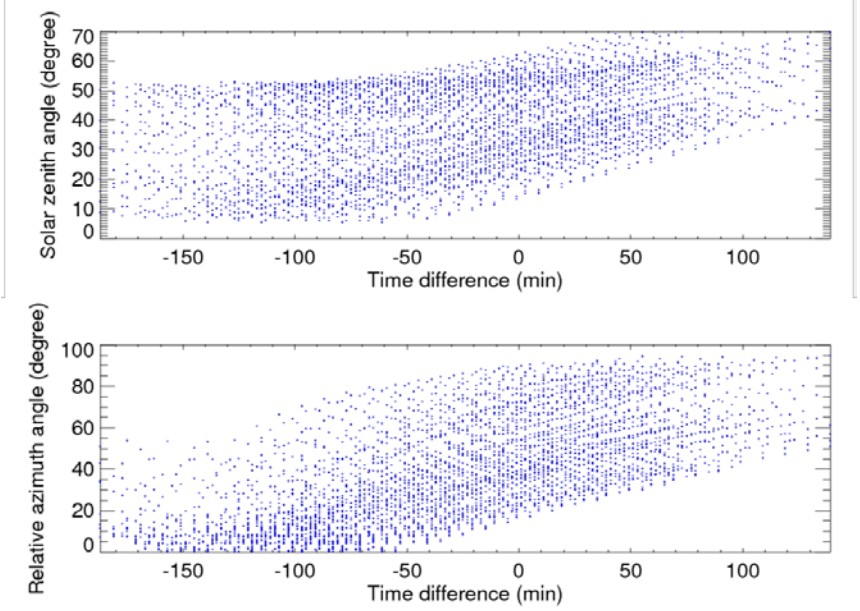

Figure 10. (Top) AHI solar zenith angle as function of measurement time difference with VIIRS measurement over the selected site for the year 2016. 24 AHI measurements are analyzed around VIIRS passing time each day. (Bottom) AHI relative azimuth angle as a function of measurement time with VIIRS for 2016 measurements over the selected site. AHI has a fixed sensor zenith angle of 33.8º.

4.3 VIIRS-AHI difference

Figure 11 shows the difference between VIIRS and AHI as function of their measurement time difference for 6 matching band pairs between AHI and VIIRS M bands and 3 matching band pairs between AHI and VIIRS I bands. The blue dots are the difference before corrections and the red dots are the difference after corrections. The difference before correction is up to 40%. The simultaneous measurements have almost the same solar zenith angle. However, the sensor zenith angle and the relative azimuth angle still impact the difference. The difference after correction is significantly

reduced to the 10% range even for large time differences. The large time difference effects include the solar angle difference and target variation such as cloud movement. The solid line is the quadratic fit of their comparison as function of time difference. A weight which is the inverse of observation time difference is applied in the fit.

The AHI-VIIRS differences around simultaneous measurements (within ±10 minutes time difference) were processed. The impact of modeling errors is reduced for simultaneous measurements since they have almost the same solar zenith angle. The difference at zero time difference using the fitting function is calculated. The fitted curve shows variation with time difference which can be attributed to modeling errors. The cloud movements can be treated as random noise of the difference. The calculated reflectance difference at zero time difference can be used to reduce the modeling errors. The modeling errors include the 6SV and BRDF modeling for VIIRS and the impact of band spectral difference when applying VIIRS modeling to AHI. Table 2 listed the differences for 6 matching band pairs. The SBAF was derived using MODTRAN modeling for a typical desert site and can introduce large uncertainty for the adjustment factors. The difference before and after the adjustment using SBAF are presented.

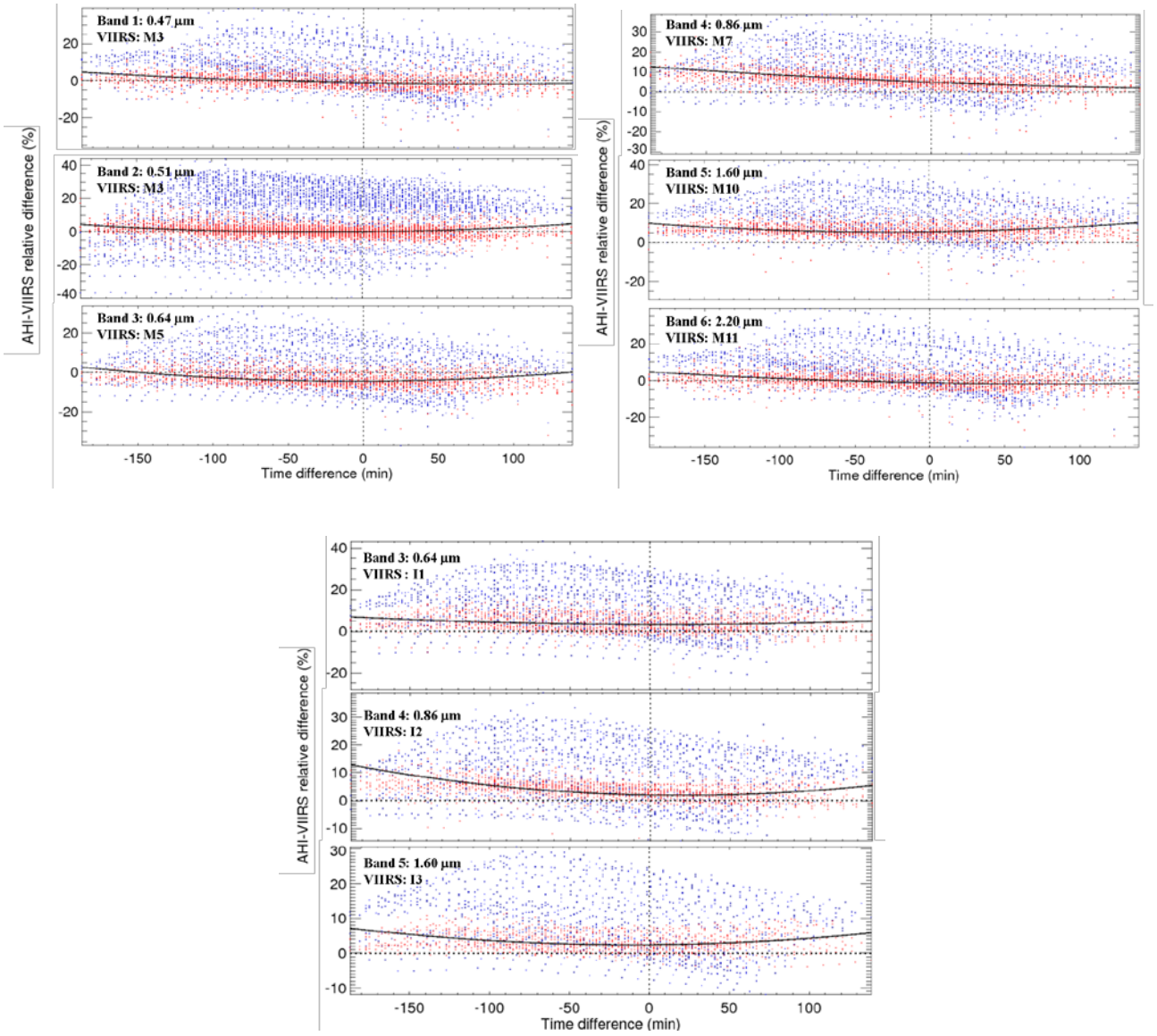

Figure 11. The difference between VIIRS and AHI as function of their measurement time difference for their 6 matching band pairs between AHI and VIIRS M bands and 3 matching band pairs between AHI and VIIRS I bands. The blue dots are the difference before corrections and the red dots are the difference after corrections. The solid line is the quadratic fit of their difference as function of time difference.

Table 2. AHI-VIIRS difference in percentage.

AHI band (μm)		0.47	0.51	0.64	0.86	1.60	2.20	0.64	0.86	1.60
VIIRS band		M3	M3	M5	M7	M10	M11	I1	I2	I3
Without SBAF	±10min time diff. (%)	-0.32	-3.35	-4.32	4.47	5.64	-1.19	3.09	2.60	2.55
	Fitted @ zero time diff. (%)	-0.15	-3.24	-4.23	3.76	5.40	-1.24	3.25	1.96	2.48
With SBAF	±10min time diff. (%)	-0.02	-3.63	0.84	4.74	5.32	-0.42	3.17	2.90	1.94
	Fitted @ zero time diff. (%)	0.15	-3.52	0.93	4.03	5.09	-0.47	3.33	2.26	1.87

5. SUMMARY

This work focuses on an inter-comparison method for RSB between GEO-LEO sensors. The Strzelecki Desert site in Australia is selected as the comparison site for its pseudo-invariance and availability in AHI data. The 6SV model is used for atmospheric correction. A semi-empirical model is used for the BRDF correction. BRDF coefficients are derived for each matching band for this site using 2016 VIIRS measurements. The BRDF coefficients are used for the correction of both AHI and VIIRS ground reflectance. The SBAF derived using MODTRAN is applied to adjust the reflectance due to band spectral difference. AHI and VIIRS differences are analyzed for 9 matching band pairs. Their measurement time dependence is analyzed for additional corrections. AHI band 1 (0.47 μm) is in good agreement with VIIRS band M3 with a difference of 0.15%. AHI band 5 (1.61 μm) shows the largest difference of 5.09% comparing with VIIRS M10, while AHI band 5 shows less difference (1.87%) in comparison with VIIRS band I3. The method developed in this work can

be applied to the inter-comparison between GOES-16/ABI, MODIS, VIIRS, and Himawari/AHI. Future work will include enhancement of the comparison accuracy and algorithm improvement.

ACKNOWLEDGMENT

The authors would like to acknowledge Amit Angal, Jeff McIntire, and Hassan Oudrari for their reviews and comments. The Himawari-8/AHI L1B data used in this study was supplied by the P-Tree System, Japan Aerospace Exploration Agency (JAXA).

REFERENCES

[1] Bessho, K., Hayashi, M., Ikeda, A., Inoue, H., Kumagai, Y., Miyakawa, T., Murata, H., Tomoo, O., Okuyama, A., Oyama, R., et al., "An introduction to himawari-8/9 japans new-generation geostationary meteorological satellites," Journal of the Meteorological Society of Japan. Ser. II 94(2), 151–183 (2016).

[2] T. J. Schmit, P. Griffith, M. M. Gunshor, J. M. Daniels, S. J. Goodman, and W. J. Lebair, "A Closer Look at the ABI on the GOES-R Series". Bull. Amer. Meteor. Soc., 98**,** 681–698, (2017)

[3] Cao, C., and A. K. Heidinger, "Intercomparison of the longwave infrared channels of MODIS and AVHRR/NOAA-16 using simultaneous nadir observations at orbit intersections". Proc. Earth Observing Systems VII, Seattle, WA, International Society for Optical Engineering, 306–316, (2002).

[4] Cao, C., M. Weinreb, and H. Xu, “Predicting simultaneous nadir overpasses among polar-orbiting meteorological satellites for intersatellite calibration of radiometers,” Journal of Atmospheric and Oceanic Technology, 21, 537-542, (2004).

[5] Yu., F. and X. Wu, “Radiometric Inter-Calibration between Himawari-8 AHI and S-NPP VIIRS for the Solar Reflective Bands”, Remote Sensing, 8(3), 165, (2016)

[6] Xiong, X., C. Cao, and G. Chander, “An overview of sensor calibration inter-comparison and applications”, Frontiers of Earth Science in China, 4(2), 237-252 (2010).

[7] Svetlana Y. Kotchenova, Eric F. Vermote, Raffaella Matarrese, and Frank J. Klemm, Jr., “Validation of a vector version of the 6S radiative transfer code for atmospheric correction of satellite data. Part I: Path radiance”, Applied Optics, 45(26), 6762–6774, (2006)

[8] Svetlana Y. Kotchenova and Eric F. Vermote, “Validation of a vector version of the 6S radiative transfer code for atmospheric correction of satellite data. Part II. Homogeneous Lambertian and anisotropic surfaces” Applied Optics, 46(20), 4455–4464, (2007)

[9] Levy, Robert C., Remer, Loraine A., and Dubovik, Oleg, “Global aerosol optical properties and application to Moderate Resolution Imaging Spectroradiometer aerosol retrieval over land”, Journal Of Geophysical Research: Atmospheres, 112, D13210, (2007)

[10] Vermote E., D. Tanré, J. L. Deuzé, M. Herman, J. J. Morcrette, and S. Y. Kotchenova, “Second Simulation of a Satellite Signal in the Solar Spectrum - Vector (6SV)”, http://6s.ltdri.org/pages/manual.html

[11] J. L. Roujean, M. J. Leroy, and P. Y. Deschamps, “A bidirectional reflectance model of the Earth’s surface for the correction of remote sensing data,” J. Geophys. Res., 97(D18), 20455–20468, (1992).

[12] P.M. Teillet, J.A. Barsi, G. Chander, and K.J. Thome, “Prime Candidate Earth Targets for the Post-Launch Radiometric Calibration of Space-Based Optical Imaging Instruments” Proc. SPIE 6677, Earth Observing Systems XII, 66770S (September 26, 2007)

[13] C. Cao, F. Deluccia, X. Xiong, R. Wolfe, and F. Weng, “Early On-orbit Performance of the Visible Infrared Imaging Radiometer Suite (VIIRS) onboard the Suomi National Polar-orbiting Partnership (Suomi-NPP) Satellite”, IEEE Transactions on Geoscience and Remote Sensing, 52(2), 1142 – 1156, (2014)

[14] X. Xiong, J. Butler, K. Chiang, B. Efremova, J. Fulbright, N. Lei, J. McIntire, H. Oudrari, J. Sun, Z. Wang, and A. Wu, “VIIRS on-orbit calibration methodology and performance”, Journal Of Geophysical Research: Atmospheres, 119, 1–11, (2014)

[15] Chander, G., Mishra, N., Helder, D.L., Aaron, D.B. “Applications of Spectral Band Adjustment Factors (SBAF) for Cross-Calibration”, IEEE Transactions on Geoscience and Remote Sensing. 51(3), 1267-1281, (2013)

[16] Scarino, B., D. R. Doelling, P. Minnis, A. Gopalan, T. Chee, R. Bhatt, C. Lukashin, and C. O. Haney, “A Web-based Tool for Calculating Spectral Band Difference Adjustment Factors Derived from SCIAMACHY Hyper-spectral Data”, IEEE Transactions on Geoscience and Remote Sensing, 54(5), 2529 – 2542, (2016)

[17] A. Berk, G. P. Anderson, P. K. Acharya, and E. P. Shettle MODTRAN 5.2.0.0 User’s Manual Air Force Res. Lab., Space Veh. Directorate, Air Force Materiel Command, Bedford, MA, USA, 01731–3010, (2008).

[18] T. Chang, X. Wu, F. Weng, "Postlaunch calibration update of MetOp-B AVHRR reflective solar channels using MetOp-A", IEEE Transactions on Geoscience and Remote Sensing, 53(5), 2286-2294, (2015)

[19] T. Chang, X. Xiong, A. Angal, A. Wu and X. Geng, "Aqua and Terra MODIS RSB Calibration Comparison Using BRDF Modeled Reflectance," IEEE Transactions on Geoscience and Remote Sensing, 55(4), 2288-2298, (2017)

Captions

Figure 2. The SRFs of the matching band pairs of AHI and VIIRS are plotted for comparison. The AHI band spectral response functions are plotted in black. Blue curves denote VIIRS M bands and red curves denote VIIRS I bands.

Figure 2. The himawari-8 location and calibration site location on map [1].

Figure 3. (Left) VIIRS solar and view angle coverage for 2016 measurements over the selected site. (Right) AHI solar angle coverage for 2016 measurements over the selected site. AHI has a fixed sensor zenith angle of 33.8 º.

Figure 4. TOA reflectance measurements from VIIRS band M3 as function of solar and view angles. The measurements are from 2016 over the selected site.

Figure 5. (Left) Rayleigh scattering as function of solar and view angles for VIIRS band M3 from one-year of measurements (2016) over the selected site. (Right) The ratio of the Rayleigh scattering to TOA reflectance for M3.

Figure 6. (Left) Ground reflectance as function of solar and view angles for VIIRS band M3 from one-year of measurements (2016) over the selected site. (Right) The ground reflectance from the BRDF model for VIIRS band M3.

Figure 7. AHI band 1 TOA reflectance measurements during 4 hour time and over the selected site. The data points in blue were identified as contaminated measurements.

Figure 8. (Left) Ground reflectance as a function of solar and view angles for VIIRS band M3 from 2016 measurements over the selected site. (Right) The BRDF corrected ground reflectance of each measurement for VIIRS M3.

Figure 9. The flow chart for corrections and comparison between VIIRS and AHI for each matching band pair.

Figure 10. (Top) AHI solar zenith angle as function of measurement time difference with VIIRS measurement over the selected site for the year 2016. 24 AHI measurements are analyzed around VIIRS passing time each day. (Bottom) AHI relative azimuth angle as a function of measurement time with VIIRS for 2016 measurements over the selected site. AHI has a fixed sensor zenith angle of 33.8º.

Figure 11. The difference between VIIRS and AHI as function of their measurement time difference for their 6 matching band pairs between AHI and VIIRS M bands and 3 matching band pairs between AHI and VIIRS I bands. The blue dots are the difference before corrections and the red dots are the difference after corrections. The solid line is the quadratic fit of their difference as function of time difference.

Biographies

Tiejun Chang received a M.S. degree in Computer Science from Montana State University, and a Ph.D degree in Optics from University of Paris-Sud, France. His work focuses on radiometric calibration and validation of satellite remote sensor and has experience on MODIS, VIIRS, AVHRR, and GOES-R/ABI. He is working with MODIS and VIIRS Characterization and Support Teams at the National Aeronautics and Space Administration (NASA), Goddard Space Flight Center (GSFC).

Xiaoxiong (Jack) Xiong received the B.S. degree in optical engineering from the Beijing Institute of Technology, Beijing, China, and the Ph.D. degree in physics from the University of Maryland, College Park.He is an optical physicist at the National Aeronautics and Space Administration (NASA), Goddard Space Flight Center (GSFC), currently serving as the MODIS Project Scientist and the Technical Lead for both the MODIS Characterization Support Team (MCST) and the VIIRS Characterization Support Team (VCST).

Graziela R. Keller received her Ph.D. degree in Astronomy from Universidade de Sao Paulo, Brazil. She is currently a Senior Research Scientist with Science Systems and Applications, Inc., Lanham, MD, USA, primarily working with calibration and characterization of the Moderate Resolution Imaging Spectroradiometer (MODIS) on board the Terra and Aqua satellites. Before joining the MODIS Characterization and Support Team (MCST), she also worked in the fields of magnetohydrodynamics of stellar winds and stellar astrophysics.

Xiangqian Wu leads calibration support for NOAA's operations of Advanced Very High Resolution Radiometer (AVHRR) on POES (since 2002), Imager and Sounder on GOES (since 2004), Ozone

Mapper Profiler Suite (OMPS) on S-NPP (2011-2014), and Advanced Baseline Imager (ABI) on GOES-R (since 2014). He has been a member of the WMO-sponsored Global Space-based Inter-Calibration System (GSICS) Research Working Group since its inception in 2006, and served as its first chair.